International Journal of Structural Stability and Dynamics
Vol. 8, No. 1 (2008) 41–60

A SIMPLE MODELING AND EXPERIMENT ON DYNAMIC STABILITY OF A DISK ROTATING IN AIR

XINGZHE WANG* and X. Y. HUANG†

*School of Civil Engineering and Mechanics
Lanzhou University, Lanzhou 730000, P. R. China
xzwang@lzu.edu.cn

†School of Mechanical and Production Engineering
Nanyang Technological University, 639798 Singapore

Received 26 March 2007
Accepted 13 August 2007

In this paper, the dynamic stability of a disk rotating in air has been modeled and analyzed numerically as well as observed from experiments. A simple expression on the aerodynamic loading acting on the rotating disk is applied in the modeling, and the dynamic stability results of the disks are evaluated based on the eigenvalues for the vibration modes. The disk critical speeds and the flutter speeds are calculated and compared with the results from experiments, which are conducted on two steel disks with different diameters and thicknesses. The modeling predicts that the rotating disk flutter starts with the mode $(0, 3)$B, which agrees with the results reported in the literature and the observation in the present experimental study.

Keywords: Rotating disks; aeroelastic instability; disk flutter; critical and flutter speeds.

1. Introduction

As the basic elements, rotating disks are widely utilized in the high capacity and performance data storage devices, such as VCDs/DVDs, floppy disk and hard disk drives of computers, as well as turbines and gyroscopes. When the rotational speed increases, the natural frequency of backward traveling wave (BTW) of a rotating disk decreases and vanishes at a critical speed, where a stationary transverse force excites resonance that causes buckling instability of the rotating disk. Another important issue to be considered is the dynamic instability of aeroelasticity of the rotating disk, that is, disk flutter. When a thin disk rotates at a high speed, it may be coupled with the air around it in such a way that the self-excited vibration can be induced and a small disturbance on some disk vibration modes will be amplified into large amplitude vibrations. The flutter of rotating disks has recently become an important research topic and active research area, stimulated by the fast development of disk-related data storage devices.[1,2]

In modeling the disk flutter, Renshaw *et al.*[3] investigated analytically and experimentally the stability of a rotating disk coupled to the surrounding fluid with an assumption of irrotational flow. The authors discussed some parameters that influence the stability of the system, but they did not give any direct numerical predictions and the comparisons with experimental observations on the flutter speed of the rotating disk. D'Angelo and Mote[4] conducted an experiment on thin disks in an enclosure with different air densities and they observed the disk flutter for the vibration mode $(0, 3)$. They reported that the flutter speed would increase with the decrease of the air density and confirmed that the flutter was induced by the aerodynamic coupling of air to the rotating disk. Lee *et al.*[5] conducted an experiment to measure the critical speeds of optical disks, and the disk flutter was detected at the $(0, 3)$ mode. The investigations on stability of floppy disks were reported by many researchers (e.g. Hosaka and Crandall,[6] Chonan *et al.*,[7] Huang and Mote,[8,9] Naganathan *et al.*[10]). In these studies, the air between the disk and the enclosure walls was modeled as a viscous film that generated a damping force on the rotating disk. They showed that the damping forces induced by the air films could lead to disk flutter at a high rotation speed. The results are generally for low gas Reynolds numbers such as those found in floppy or zip disk applications.

In the study of rotating disk flutter, the key issue is the aerodynamic loading of the air spinning around the rotating disk. Some empirical models have been proposed to relate the disk vibrations to the air pressure loadings. Several researchers used a rotating damping model to predict flutter in enclosed and unenclosed disks.[6,11] Some researchers utilized discrete springs to model the acoustic coupling between disks in disk stacks.[12,13] These models may be appropriate for explaining instability and certain vibration coupling phenomena in the rotating disk systems, but these models are not entirely predictive in the sense due to some coefficients in the models having to be determined experimentally. Yasuda *et al.*[14] suggested an expression for the aerodynamic force acting on a disk spinning in an infinite medium which was formulated in terms of "damping" and "lift" forces. They assumed that the ratio between the lift and damping forces was proportional to the disk rotation speed, and showed that flutter could occur at a certain rotation speed. The expression of aerodynamic force was further developed by Kim *et al.*[15] and Hansen *et al.*[16] in an aeroelastic model to include a series of parameters $(S_{mn}, c_{mn}, \Omega'_{dmn})$ determined for each mode (m, n) and rotation speed. The parameters in the aeroelastic model, however, were highly dependent on the viscosity of the fluid, the disk rotation speed, the disk-enclosure configuration and frequencies of each disk mode (m, n) for forward traveling wave (FTW) and BTW. The determination of these parameters for each mode at each rotation speed may limit the application of the model in practice. Besides, there is no report on a direct comparison of predictions based on this model with experimental observations in terms of the flutter speed and the flutter mode. There may be a need to simplify the aeroelastic model and to verify the flutter prediction by experiments, which motivated the present study.

In this paper, both numerical simulations and experimental observation have been carried out on disks rotating between two rigid plates. A simple aeroelastic model is proposed on the basis of the work of Kim *et al.*[15] and Hansen *et al.*[16] The model replaces the coefficient operators with some nondimensional constants independent of each mode of the rotating disk, and has been applied in the disk motion equation to predict the critical and flutter speeds. The results are compared with the experimental observations to show reasonable agreements.

2. Numerical Modeling

2.1. *Fundamental equations*

Consider a thin disk rotating between two stationary circular plates, which have a radius r_e and are placed a distance $2z_e$ apart as shown in Fig. 1. The disk has a uniform thickness h, outer radius r_{o}, and clamped at the center with the radius r_i. The Young's modulus, the Poisson ratio, and the density of the disk are respectively E, ν and ρ_{d}, and the density of the air is ρ_{a}. The material damping of the disk is normally very small, and thus it is assumed to be negligible in the present study. The disk rotates at a constant angular speed Ω. A stationary coordinate system (r, θ, z) is used in the modeling. The rotating disk with small transverse motions is modeled with the linear Kirchhoff's plate theory. The governing equation for the vibration of the disk with the membrane stresses induced by the rotation and the aerodynamic loading $f(r, \theta, t)$ can be written as

$$\rho_{\mathrm{d}} h \left(\frac{\partial^2 w}{\partial t^2} + 2\Omega \frac{\partial^2 w}{\partial t \partial \theta} + \Omega^2 \frac{\partial^2 w}{\partial \theta^2} \right) + D\nabla^4 w - h \left[\frac{1}{r} \frac{\partial}{\partial r} \left(r\sigma_r \frac{\partial w}{\partial r} \right) + \frac{1}{r^2} \frac{\partial}{\partial \theta} \left(\sigma_\theta \frac{\partial w}{\partial \theta} \right) \right] = f(r, \theta, t), \quad (1)$$

where $w(r, \theta, t)$ is the transverse displacement of the disk, $D = Eh^3/\lfloor 12(1-\nu^2) \rfloor$ is the bending rigidity of the disk, $\nabla^4 = (\frac{\partial^2}{\partial r^2} + \frac{\partial}{r\partial r} + \frac{\partial^2}{r^2 \partial \theta^2})^2$ is the biharmonic differential operator, σ_r and σ_θ are the radial and hoop membrane stresses, respectively,

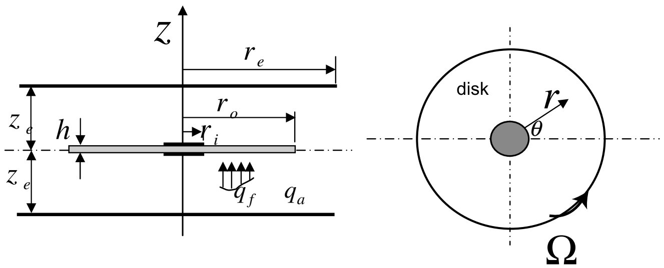

Fig. 1. The geometry of a disk rotating between two plates.

and are given by[3]:

$$\sigma_r = \rho_{\mathrm{d}} r_{\mathrm{o}}^2 \Omega^2 \left[b_0 \left(\frac{r_{\mathrm{o}}}{r}\right)^2 + b_1 - \frac{3+\nu}{8}\left(\frac{r}{r_{\mathrm{o}}}\right)^2 \right],$$

$$\sigma_\theta = \rho_{\mathrm{d}} r_{\mathrm{o}}^2 \Omega^2 \left[-b_0 \left(\frac{r_{\mathrm{o}}}{r}\right)^2 + b_1 - \frac{1+3\nu}{8}\left(\frac{r}{r_{\mathrm{o}}}\right)^2 \right], \tag{2}$$

in which

$$\begin{aligned} b_0 &= \frac{(1-\nu)(r_i/r_{\mathrm{o}})^2[(3+\nu)-(1+\nu)(r_i/r_{\mathrm{o}})^2]}{8[(1+\nu)+(1-\nu)(r_i/r_{\mathrm{o}})^2]}, \\ b_1 &= \frac{(1+\nu)[(3+\nu)+(1-\nu)(r_i/r_{\mathrm{o}})^4]}{8[(1+\nu)+(1-\nu)(r_i/r_{\mathrm{o}})^2]}. \end{aligned} \tag{3}$$

The boundary conditions for the disk, which is clamped by a collar ($r = r_i$) and free at its rim ($r = r_{\mathrm{o}}$) where the bending moment and shearing force components vanish, are respectively given by

$$w|_{r=r_i} = 0, \quad \left.\frac{\partial w}{\partial r}\right|_{r=r_i} = 0, \tag{4}$$

$$\begin{aligned} \left[\frac{\partial^2 w}{\partial r^2} + \nu\left(\frac{1}{r}\frac{\partial w}{\partial r} + \frac{1}{r^2}\frac{\partial^2 w}{\partial \theta^2}\right)\right]_{r=r_{\mathrm{o}}} &= 0, \\ \left[\frac{\partial}{\partial r}(\nabla^2 w) + \frac{(1-\nu)}{r^2}\frac{\partial^2}{\partial \theta^2}\left(\frac{\partial w}{\partial r} - \frac{w}{r}\right)\right]_{r=r_{\mathrm{o}}} &= 0. \end{aligned} \tag{5}$$

The hydrodynamic model, based on the rigorous Navier–Stokes equations, for the description of the aerodynamic force, $f(r,\theta,t)$, arising from the airflow of the disk rotation is highly complicated to provide an analytical design. Here, we take the surrounding fluid of the rotating disk influencing on the disk behavior as the contributions from irrotational flow and rotational flow components. Consequently, the aerodynamic loading $f(r,\theta,t)$ may be divided into two parts, $q_{\mathrm{a}}(r,\theta,t)$ and $q_{\mathrm{f}}(r,\theta,t)$. The first part, $q_{\mathrm{a}}(r,\theta,t)$, is the acoustic pressure between the upper and lower surfaces of the disk, which is induced from the disk vibration without considering rotation effect, i.e. the contribution from irrotational flow. This part was adopted in Renshaw *et al.*'s study.[3] The second part, $q_{\mathrm{f}}(r,\theta,t)$, is the aerodynamic force arising from the vortex airflow due to the disk rotation, i.e. the contribution from rotational flow. It is clear that $q_{\mathrm{f}}(r,\theta,t)$ is equal to zero if the disk does not rotate while $q_{\mathrm{a}}(r,\theta,t)$ will always be there as long as the disk vibrates in air.

The acoustic force $q_{\mathrm{a}}(r,\theta,t)$ on the disk can be calculated through the pressure difference between the upper ($z = 0^+$) and lower ($z = 0^-$) surfaces of the disk, and can be written as[3]:

$$q_{\mathrm{a}}(r,\theta,t) = \rho_{\mathrm{a}}\left(\left.\frac{\partial \phi_{\mathrm{a}}(r,\theta,z,t)}{\partial t}\right|_{z=0^+} - \left.\frac{\partial \phi_{\mathrm{a}}(r,\theta,z,t)}{\partial t}\right|_{z=0^-} \right), \tag{6}$$

in which ϕ_{a} is the acoustic velocity potential. The governing equation for the acoustic field surrounding the disk is expressed by

$$\nabla^2\phi_{\mathrm{a}} = \frac{1}{a^2}\frac{\partial^2\phi_{\mathrm{a}}}{\partial t^2}, \tag{7}$$

where a is the speed of sound, ∇^2 is the space Laplacian operator. The boundary conditions for ϕ_{a} are

$$\phi_{\mathrm{a}}|_{r=r_e} = 0, \qquad \left.\frac{\partial\phi_{\mathrm{a}}}{\partial z}\right|_{z=\pm z_e} = 0. \tag{8}$$

In addition, on the surface of disk, the acoustic velocity should match the disk vibration velocity, and at the clearance between the disk rim and the side, $\phi_{\mathrm{a}} = 0$ for the asymmetric acoustics field. So that we have the following condition:

$$\left.\frac{\partial\phi_{\mathrm{a}}}{\partial z}\right|_{z=0} = \begin{cases} 0 & (0 \le r < r_i) \\ \frac{\partial w}{\partial t} & (r_i \le r \le r_{\mathrm{o}}) \end{cases} \quad \text{and} \quad \phi_{\mathrm{a}}|_{z=0} = 0, \quad (r_{\mathrm{o}} < r \le r_e). \tag{9}$$

As for the second part of aerodynamic loading, the empirical model generalized by Kim *et al.*[15] and Hansen *et al.*[16] is employed in the present study for the aerodynamic force $q_{\mathrm{f}}(r,\theta,t)$, and it has the form of

$$q_{\mathrm{f}}(r,\theta,t) = -C_{\mathrm{d}}\left[\frac{\partial w}{\partial t} + (\Omega - \Omega_{\mathrm{d}})\frac{\partial w}{\partial\theta}\right], \tag{10}$$

where C_{d} is a damping coefficient. In general, C_{d} is an unknown self-joint operator, and Ω_{d} is the rotation speed of the distributed viscous damping force relative to the disk. Both of them are dependent on the viscous of the fluid, the disk rotation speed, the disk-enclosure configuration, and frequencies of each disk mode (m,n). We will later simplify the aerodynamic force of this model for analysis.

In the following analysis, the variables are normalized by $r_{\mathrm{o}}, h, \rho_{\mathrm{d}}$, and Ω,

$$\begin{gathered} \bar{r} = \frac{r}{r_{\mathrm{o}}}, \quad \bar{z} = \frac{z}{r_{\mathrm{o}}}, \quad \bar{t} = \Omega t, \quad \bar{w} = \frac{w}{h}, \quad \kappa = \frac{r_i}{r_{\mathrm{o}}}, \quad \bar{r}_e = \frac{r_e}{r_{\mathrm{o}}}, \\ \bar{\sigma}_r = \frac{\sigma_r}{\rho_{\mathrm{d}} r_{\mathrm{o}}^2\Omega^2}, \quad \bar{\sigma}_\theta = \frac{\sigma_\theta}{\rho_{\mathrm{d}} r_{\mathrm{o}}^2\Omega^2}, \quad \bar{q}_{\mathrm{f}} = \frac{q_{\mathrm{f}}}{\rho_{\mathrm{d}} h^2\Omega^2}, \quad \bar{q}_{\mathrm{a}} = \frac{q_{\mathrm{a}}}{\rho_{\mathrm{d}} h^2\Omega^2}, \quad \bar{\phi}_{\mathrm{a}} = \frac{\phi_{\mathrm{a}}}{r_{\mathrm{o}} h\Omega}. \end{gathered} \tag{11}$$

By using the above nondimensional parameters, all foregoing equations can be rewritten in dimensionless forms. We will drop the bars on the variables in the following analysis for simplicity and convenience without a risk of confusion. Thus, we have the equation for vibration of the rotating disk

$$\begin{aligned} &\frac{\partial^2 w}{\partial t^2} + 2\frac{\partial^2 w}{\partial t\partial\theta} + \frac{\partial^2 w}{\partial\theta^2} + \varepsilon\nabla^4 w - \left[\frac{1}{r}\frac{\partial}{\partial r}\left(r\sigma_r\frac{\partial w}{\partial r}\right) + \frac{1}{r^2}\frac{\partial}{\partial\theta}\left(\sigma_\theta\frac{\partial w}{\partial\theta}\right)\right] \\ &\quad = \Lambda\left[\frac{\partial\phi_{\mathrm{a}}(r,\theta,z=0^+,t)}{\partial t} - \frac{\partial\phi_{\mathrm{a}}(r,\theta,z=0^-,t)}{\partial t}\right] - C\left[\frac{\partial w}{\partial t} + \left(1 - \frac{\Omega_{\mathrm{d}}}{\Omega}\right)\frac{\partial w}{\partial\theta}\right] \end{aligned} \tag{12}$$

and the boundary conditions

$$w|_{r=\kappa} = 0, \quad \left.\frac{\partial w}{\partial r}\right|_{r=\kappa} = 0, \tag{13}$$

$$\left[\frac{\partial^2 w}{\partial r^2} + \nu\left(\frac{1}{r}\frac{\partial w}{\partial r} + \frac{1}{r^2}\frac{\partial^2 w}{\partial \theta^2}\right)\right]_{r=1} = 0,$$

$$\left[\frac{\partial}{\partial r}(\nabla^2 w) + \frac{(1-\nu)}{r^2}\frac{\partial^2}{\partial \theta^2}\left(\frac{\partial w}{\partial r} - \frac{w}{r}\right)\right]_{r=1} = 0. \tag{14}$$

In Eq. (12), $\varepsilon = \frac{D}{\rho_{\mathrm{d}} r_{\mathrm{o}}^4 h \Omega^2} = \frac{1}{6(1-\nu)}(\frac{c_s}{r_0\Omega})^2(\frac{h}{r_0})^2$ is the ratio of the bending stiffness of the disk to the stiffness derived from the centrifugal body force, where $c_{\mathrm{s}} = \sqrt{\frac{E}{2(1+\nu)}}$ is the shear wave speed, $r_0\Omega$ is the linear speed of rotation. $\Lambda = \frac{\rho_{\mathrm{a}} r_{\mathrm{o}}}{\rho_{\mathrm{d}} h}$ is the ratio of the densities of the airflow and the disk. In the last term at right hand of Eq. (12), the expression for the nondimensional form of aeroelastic force is characterized and simplified here by two nondimensional parameters of real numbers, that is, $C = \frac{C_{\mathrm{d}}}{\rho_{\mathrm{d}} h \Omega}$ for the ratio of aerodynamic damping and $\frac{\Omega_{\mathrm{d}}}{\Omega}$ for the ratio of damping speed.

The equation for the acoustic field

$$\nabla^2 \phi_{\mathrm{a}} = M^2 \frac{\partial^2 \phi_{\mathrm{a}}}{\partial t^2} \tag{15}$$

and the boundary conditions

$$\phi_{\mathrm{a}}|_{r=r_e} = 0, \quad \left.\frac{\partial \phi_{\mathrm{a}}}{\partial z}\right|_{z=\pm z_e} = 0, \tag{16}$$

where $M = r_{\mathrm{o}}\Omega/a$ is the Mach number at the outer edge of the disk. The match conditions on the disk surface and at the clearance between the disk rim and the side become

$$\left.\frac{\partial \phi_{\mathrm{a}}}{\partial z}\right|_{z=0} = \begin{cases} 0 & (0 \le r < \kappa) \\ \dfrac{\partial w}{\partial t} & (\kappa \le r \le 1) \end{cases} \quad \text{and} \quad \phi_{\mathrm{a}}|_{z=0} = 0, \quad (1 < r \le r_e). \tag{17}$$

Equations (12) and (15), together with the boundary conditions, form a stability problem for the system of the rotating disk coupled with the surrounding air-flow. If the amplitude of the disk vibration w grows with time, the system is unstable and the flutter happens.

2.2. *Method of analysis*

In order to solve the air-coupled disk vibration equations, we employ an approximation method and assume the transverse displacement $w(r,\theta,t)$ and the acoustic field $\phi_{\mathrm{a}}(r,\theta,z,t)$ are of the forms

$$w(r,\theta,t) = R(r)e^{i(n\theta+\lambda t)}, \quad \phi_{\mathrm{a}}(r,\theta,z,t) = \psi_{\mathrm{a}}(r,z)e^{i(n\theta+\lambda t)}, \tag{18}$$

where $R(r)$ and $\psi_{\mathrm{a}}(r,z)$ are unknown functions to be determined. λ is the eigenvalue whose real part determines the disk vibration frequency and the imaginary part indicates the stability of the system. Function $R(r)$ can be approximated by a superposition of some linearly independent polynomials R_{mn} (Chonan *et al.*[17]):

$$\begin{aligned}R_{mn}(r) &= r^m + r^{m+1} + E_{mn}^{(1)} r^{m+2} + E_{mn}^{(2)} r^{m+3} \\ &\quad + r^{m+4} + E_{mn}^{(3)} r^{m+5} + E_{mn}^{(4)} r^{m+6},\end{aligned} \tag{19}$$

where $E_{mn}^{(i)}$ $(i = 1, 2, 3, 4)$ are constants to be determined such that all the boundary conditions of the disk are satisfied, m and n represent the numbers of nodal circle and diameter of the mode (m, n). The transverse deflections of the disk can be written as

$$w(r, \theta, t) = \sum_{m=0}^{M_0} c_m R_{mn}(r) e^{i(n\theta + \lambda t)}, \tag{20}$$

where c_m are coefficients, M_0 is an integer depending on accuracy of the modeling. The acoustic velocity potential ϕ_{a} is solved according to the boundary conditions and has the following form[3]:

$$\phi_{\mathrm{a}}(r, \theta, z, t) = \sum_{k=1}^{\infty} d_k^{\mathrm{a}} \cosh[\alpha_k (z_e - z)] J_n(\xi_k r) e^{i(n\theta + \lambda t)}, \tag{21}$$

where $J_n(\xi_k r)$ is the Bessel function of the nth order, ξ_k is determined by the roots of $J_n(\xi_k r_e) = 0$ $(k = 1, 2, \ldots, \infty)$, $\alpha_k = \sqrt{\xi_k^2 - M^2\lambda^2}$. d_k^{a} can be determined by the match condition of Eq. (17) at $z = 0$.

For two arbitrary complex-valued functions, $a(r, \theta)$ and $b(r, \theta)$, defined in the domain $\{\kappa \le r \le 1, 0 \le \theta \le 2\pi\}$, we introduce an inner product as follows:

$$\langle a(r, \theta), b(r, \theta)\rangle = \int_0^{2\pi} \int_\kappa^1 a(r, \theta) b^*(r, \theta) r dr d\theta, \tag{22}$$

where the superscript asterisk denotes the complex conjugation. By substituting Eqs. (20) and (21) into the equation of motion (12) of the disk, and then calculating the inner product with $R_{\mathrm{ln}}(r) e^{i(n\theta + \lambda t)}$, $(l = 0, 1, \ldots, M_0)$, one obtains a matrix equation for the coefficients c_m following the Galerkin's method

$$\{[\mathbf{B}] + [\mathbf{P}^{\mathrm{a}}] + [\mathbf{P}^{\mathrm{f}}]\}[\mathbf{c}] = [\mathbf{0}]. \tag{23}$$

In Eq. (23), $[\mathbf{c}] = [c_0 \quad c_1 \quad \cdots \quad c_{M_0}]^{\mathrm{T}}$, $[\mathbf{B}]$ is a $(M_0 + 1) \times (M_0 + 1)$ matrix associated with the free vibration of the rotating disk without any aerodynamic loading, $[\mathbf{P}^{\mathrm{a}}]$ is a $(M_0 + 1) \times (M_0 + 1)$ matrix associated with the acoustic force, which is evaluated in the appendix, $[\mathbf{P}^{\mathrm{f}}]$ is a $(M_0 + 1) \times (M_0 + 1)$ matrix associated with aerodynamic force due to the disk rotation. The elements for $[\mathbf{B}]$ and $[\mathbf{P}^{\mathrm{f}}]$ are given as follows:

$$B_{ml} = 2\pi \int_\kappa^1 \left[(\lambda + n)^2 R_{mn}(r) - \varepsilon \nabla_n^4 R_{mn}(r) + \frac{1}{r}\left(r\sigma_r \frac{dR_{mn}}{dr}\right) - \frac{n^2}{r^2}\sigma_\theta R_{mn}(r)\right] R_{\mathrm{ln}}(r) r dr, \tag{24}$$

$$P_{ml}^{\mathrm{f}} = -2\pi \int_\kappa^1 Ci \left[\lambda + \left(1 - \frac{\Omega_{\mathrm{d}}}{\Omega}\right) n\right] R_{mn}(r) R_{\mathrm{ln}}(r) r dr, \tag{25}$$

where $\nabla_n^4 = (\frac{d^2}{dr^2} + \frac{d}{rdr} - \frac{n^2}{r^2})^2$. The condition of nontrivial solutions for Eq. (23) leads to a characteristic equation

$$\det\{[\mathbf{B}] + [\mathbf{P}^{\mathrm{a}}] + [\mathbf{P}^{\mathrm{f}}]\} = 0 \tag{26}$$

from which the eigenvalue λ is obtained by the roots. These roots come in $(M_0 + 1)$ pairs and generate $(M_0 + 1)$ pairs of eigenvalues for a fixed nodal diameter n. The two eigenvalues in each pair are different. One corresponds to the FTW along the rotation direction of the disk, denoted by λ^{FTW}, and the other corresponds to the BTW against the rotation direction of the disk, denoted by λ^{BTW}. The real parts of the eigenvalues, $\mathrm{Re}(\lambda)$, are related to the disk vibration mode frequencies. While the imaginary parts, $\mathrm{Im}(\lambda)$, are related to the "damping" of the disk vibration, especially $\mathrm{Im}(\lambda) < 0$ indicates a self-excited vibration or the rotating flutter. When the rotation speed Ω is zero the dynamic loading will vanish, and the eigenvalues for all modes are single values, which are the disk mode frequencies. As the rotation speed is increased, the frequency of FTW will increase, whereas the frequency of BTW will initially decrease for the observers at a fixed frame. As the frequency of BTW reduces to zero, one can get the critical speed for buckling instability of the rotating disk. If the disk rotates in a vacuum, all the eigenvalues are real numbers and the system is, therefore, stable. If the disk rotates in air, the eigenvalues will be complex numbers and $\mathrm{Im}(\lambda)$ may become negative for some modes, i.e. the flutter may occur at these modes. The rotation speed, at which disk flutter sets in, is called the flutter speed.

3. Experimental Setup

The experimental setup is illustrated in Fig. 2. It consists of disks with a driving system, a disk vibration measurement, and analysis system. Two steel disks, made of 8660 steel, were used in the experiment. Disk-1 has a thickness of 0.29 mm

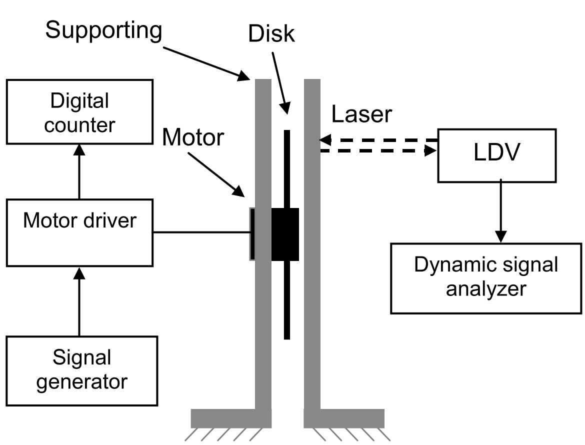

Fig. 2. Experimental setup for the measurement of disk vibrations.

and diameter of 135 mm while Disk-2 has a thickness of 0.26 mm and diameter of 100 mm. Both disks have a 25 mm diameter hole at their centers for attachment to the driving motor, and were clamped by a clamping collar and a supporting collar of diameter 31 mm. The motor was a standard motor used in commercial hard disk drives, and was driven by a motor control board together with a square wave generator. The motor rotation speed can be varied from a few hundred rpm up to 15 K rpm (revolution per minute), and was monitored by a digital counter. The disk and the motor were held between two solid plates of 160 mm in height and 240 mm in width. The space between the plates was 14 mm. The disks were mounted halfway between the plates. The front plate was made of 5 mm Perspex so that the laser beam can go in/out for the disk vibration measurement. The disk vibrations were measured by a Laser-Doppler Vibrometer (Ometron VPI Sensor) and the output signals were analyzed by a HP digital signal analyzer to obtain the spectra and waterfall plots of the disk vibrations. Apart from the disk vibrations, the output signals from the laser sensor also contained components associated with the disk rotations.

4. Results and Discussions

The results are produced and discussed for the various disk critical speeds and flutter speeds. The material and the geometric parameters for the disks used in both the simulations and the experiment are listed in Table 1. The other parameters, such as the density of air and speed of sound in air, are $\rho_{\mathrm{a}} = 1.21\,\mathrm{kg/m}^3$ and $a = 340\,\mathrm{m/s}$, respectively. Our simulations indicate that the disk flutter speed is very sensitive to the damping speed ratio $\Omega_{\mathrm{d}}/\Omega$ in Eq. (12), but the speed is not sensitive to the coefficient C. In order to avoid the difficulty of direct measurement on the damping speed ratio in the experiment, we set $\Omega_{\mathrm{d}}/\Omega = 0.85$ according to the measured flutter speed on Disk-1, and used this value to predict the flutter speed for Disk-2. The coefficient C was set as $C = 0.01$, by considering the loading term as a kind of aerodynamic "damping", and it should be light when compared to the disk material damping which is of order of 0.01–0.1.[18]

4.1. *Mode frequencies and critical speeds*

Here, we take a close view on the rotating disk behaviors of mode frequency and critical speed. In the modeling, the eigenvalues of the rotating disk are evaluated

Table 1. Geometrical and material properties of disk specimens.

Parameter	Disk-1	Disk-2
Outer diameter (mm)	135	100
Clamp diameter (mm)	31	31
Thickness (mm)	0.29	0.26
Density (kg/m^3)	7840	7840
Young's modulus (GPa)	200	200
Poisson ratio	0.3	0.3

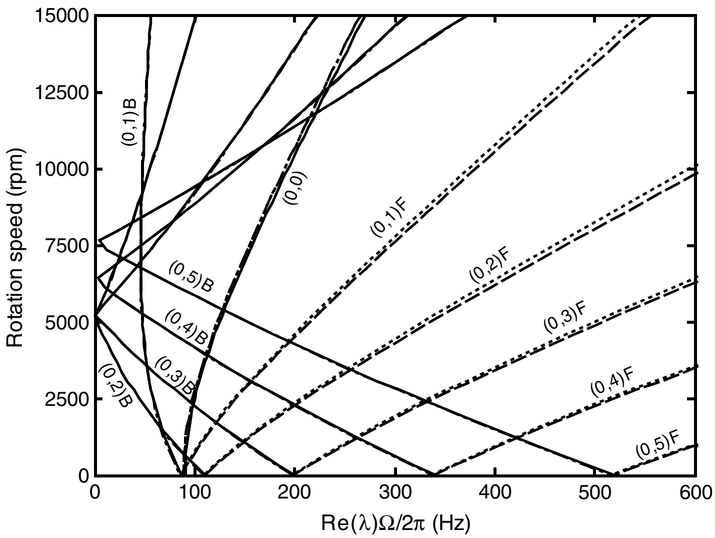

Fig. 3. Mode frequency against the rotation speed for Disk-1. The mode numbers (m, n) are indicated by the brackets and FTW and BTW are denoted by F and B, respectively. ($C = 0.01$ and $\Omega_{\rm d}/\Omega = 0.85$. Without acoustic force $q_{\rm a}$: — BTW, −− FTW; with $q_{\rm a}$: −·− BTW, ··· FTW).

for each mode and the real parts of these eigenvalues correspond to the mode frequencies. The simulations of the eigenvalues for disks are performed with allowance for the acoustic force (i.e. $q_{\rm a} \neq 0$) as well as without considering the acoustic force (i.e. $q_{\rm a} = 0$). The real parts of the eigenvalues for Disk-1 are plotted in Fig. 3. For Disk-2, the simulations are similar to the ones of Disk-1. It can be seen from Fig. 3 that the frequencies for all FTW modes increase with respect to the rotation speed. On the other hand, the frequencies for BTW modes initially decrease with the rotation speed, then reach a critical speed (zero frequency), and increase beyond that speed. The critical speed differs from one mode to another; an exception is mode $(0, 1)$B, which has no critical speed. When the rotation speed is zero (i.e. the disk does not rotate), the FTW modes and BTW modes have the same frequencies which are normal mode frequencies as observed for a stationary disk and can be obtained from Fig. 3. It can also be seen that the acoustic force in the modeling has negligible effect on the mode frequencies of BTW for the disk, except for frequencies of $(0, 0)$ mode and FTW modes. To further study the effect of acoustic force on mode frequency of the rotating disk, simulations are conducted for various geometrical parameters relating to the acoustic field in a large range of $0.01 < z_e < 2$ and $1.1 < r_e < 2$. The results are shown in Fig. 3. The acoustic force almost does not affect the mode frequencies of BTWs; and the maximums of relative difference on the mode frequencies of FTWs between the acoustic force inclusion and exclusion are less than 2% even at higher disk rotating speeds. Since buckling instability of the rotating disk is related to the BTW modes, it implies that the acoustic force has little effect on the critical speeds.

Table 2. Mode frequencies (Hz) of stationary disks.

Vibration Mode	Disk-1			Disk-2		
	Predicted Result	Measured Result	Relative Error (%)	Predicted Result	Measured Result	Relative Error (%)
$(0,0)$	87.0	77	12.9	173.3	146	18.7
$(0,1)$	83.1	73	13.8	171.2	143	19.7
$(0,2)$	107.1	108	−0.83	206.5	204	1.2
$(0,3)$	198.0	213	−7.0	338.9	352	−3.7
$(0,4)$	339.1	358	−5.3	559.8	572	−2.1
$(0,5)$	518.8	536	−3.2	849.5	852	−0.3
$(0,6)$	733.6	754	−2.7	1199.2	1186	1.1

The mode frequencies for the disks at the stationary state were measured by lightly taping the disks and recording the response spectra. The results are listed in Table 2 and are compared with the calculated values. The errors are acceptable for high modes $(0,2)$ and above, but errors are quite large for low modes $(0,0)$ and $(0,1)$. These errors were also reported by others (e.g. D'Angelo and Mote[4]), and are probably produced by imperfections in clamping at the center of the disks and non-uniform thickness of the disk. The errors for the low modes, however, will not have much effect on the following studies on the critical speeds and the flutter speeds, which are all associated with high modes. In order to measure the critical speeds, waterfall plots were generated for both disks. At each rotation speed, the disks were lightly tapped to excite the vibration modes. The plot for Disk-2 is shown in Fig. 4. The calculated BTW mode frequencies varying with rotation speeds are compared with the measured results and are shown in Figs. 5(a) and 5(b). It can

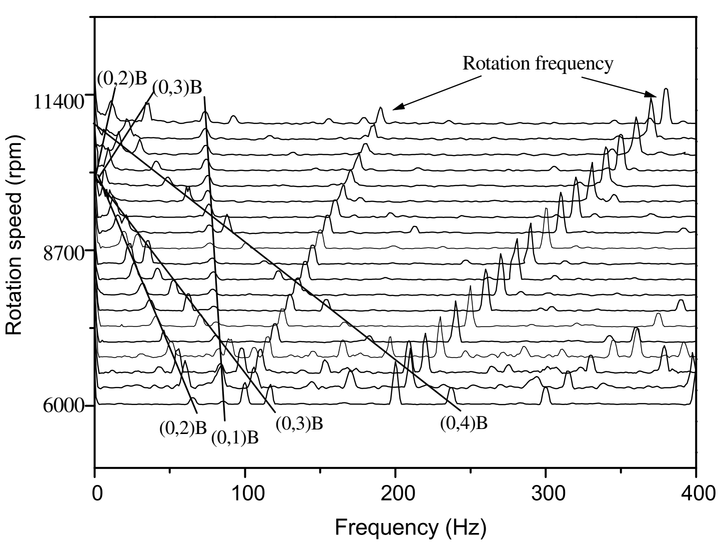

Fig. 4. Waterfall plot for Disk-2 to show the BTW mode frequencies varying with the rotation speeds.

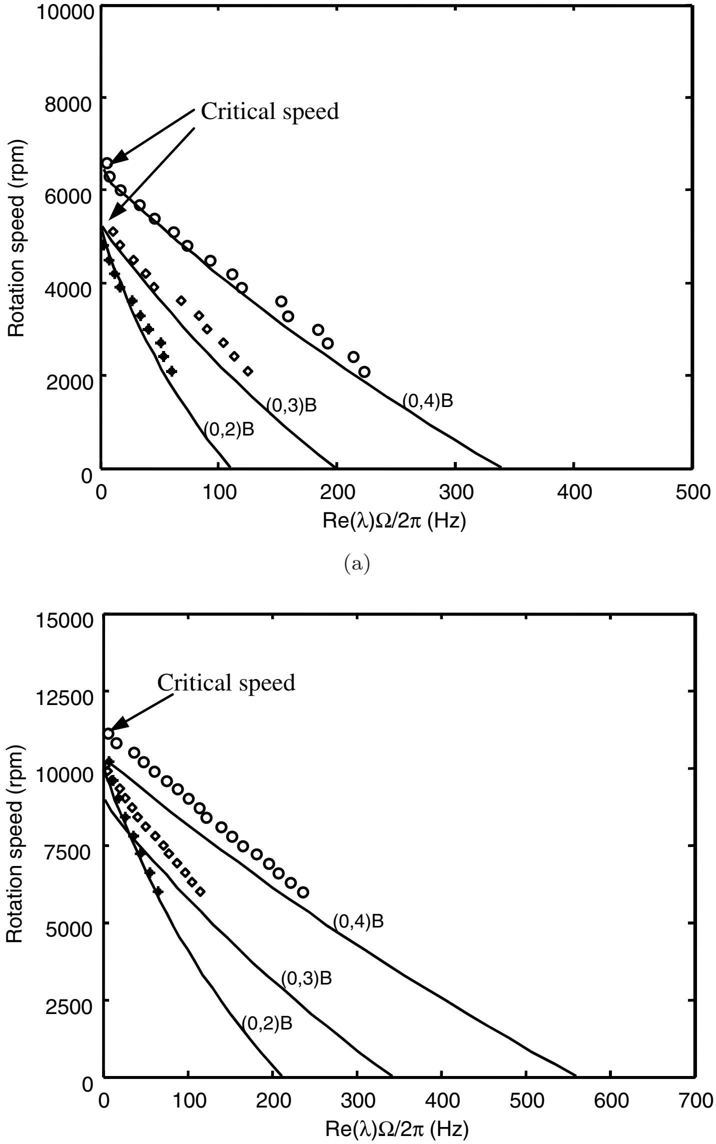

(b)

Fig. 5. Comparisons of calculated mode frequencies with experimental results for (a) Disk-1 and (b) Disk-2. The solid lines are calculated values and the scattered points are experimental data.

be seen that the measured mode frequencies, denoted by the scattered data points, follow well the modeling curves denoted by the solid lines, especially for Disk-1. The calculated critical speeds are compared with the values estimated from the experiment for modes $(0,2)$B, $(0,3)$B and $(0,4)$B shown in Table 3. The predicted critical speeds are seen to be close to the measured values for both disks.

Table 3. Critical speeds (rpm) of BTW modes.

Vibration Mode	Disk-1			Disk-2		
	Predicted Result	Measured Result	Relative Error	Predicted Result	Measured Result	Relative Error
$(0,2)$B	5200	∼5400	−3.7%	10000	∼10200	−2.0%
$(0,3)$B	5300	∼5700	−7.0%	9000	∼10100	−10.9%
$(0,4)$B	6400	∼6700	−4.5%	10500	∼11100	−5.4%

4.2. *Flutter speeds*

The flutter speeds were determined according to the imaginary part of the mode eigenvalues. We first give the flutter predictions based on the aerodynamic loading only containing acoustic force q_{a} (i.e. $q_{\mathrm{a}} \neq 0, q_{\mathrm{f}} = 0$) for Disk-1 and Disk-2. The simulation results show that the imaginary part of the mode eigenvalues are almost null which implies the non-occurrence of flutter if the acoustic force term only is considered in the modeling. By taking into account the second part (i.e. $q_{\mathrm{f}} \neq 0$) of the aerodynamic loading in the modeling, Figs. 6(a) and 6(b) show the plot of $\mathrm{Im}(\lambda)$ for both FTW and BTW modes against the rotation speed for Disk-1 and Disk-2. It can be seen that $\mathrm{Im}(\lambda)$ for all FTW modes are positive in the speed range, indicating that these modes are always stable. The modes $(0,0)$B and $(0,1)$B are also stable. The imaginary parts of the eigenvalues for other BTW modes, however, are initially positive and then switch to negative as the rotation speed increases. $\mathrm{Im}(\lambda) < 0$ means that the disks are unstable, as the vibration magnitudes will grow with time and eventually flutter occurs. The speed at which $\mathrm{Im}(\lambda)$ is moving across zero from positive to negative is defined as the flutter speed. It is seen from Fig. 6 that the flutter occurs first to mode $(0,3)$B for both disks, which was also observed and reported by D'Angelo and Mote[4] and Lee *et al.*[5] The disk flutter was observed in the present experiment by the waterfall plots for the rotation speed up to 9600 rpm for Disk-1 and 14,700 rpm for Disk-2 as shown in Figs. 7(a) and 7(b), respectively. Large amplitude vibrations are seen at high rotation speeds, which are disk flutters and are likely associated with mode $(0,3)$B. The flutter speeds are also estimated from these plots, with errors about ±300 rpm. The flutter speeds and frequencies calculated from the modeling for mode $(0,3)$B are compared with the estimated flutter speeds and frequencies based on the experimental observations in Table 4.

4.3. *Discussion on flutter modeling*

The predicted flutter speeds are sensitive to the damping speed ratio $\Omega_{\mathrm{d}}/\Omega$, which is adjusted in the calculation so that the predicted flutter speeds are close to the experimental values for one of the disks. However, since the predicted flutters agree well with the experimental observations, including the mode frequencies, the critical speeds and the flutter speeds, for both disks with different diameters and thicknesses, the comparison in Table 4 can be considered valid, thereby verifying

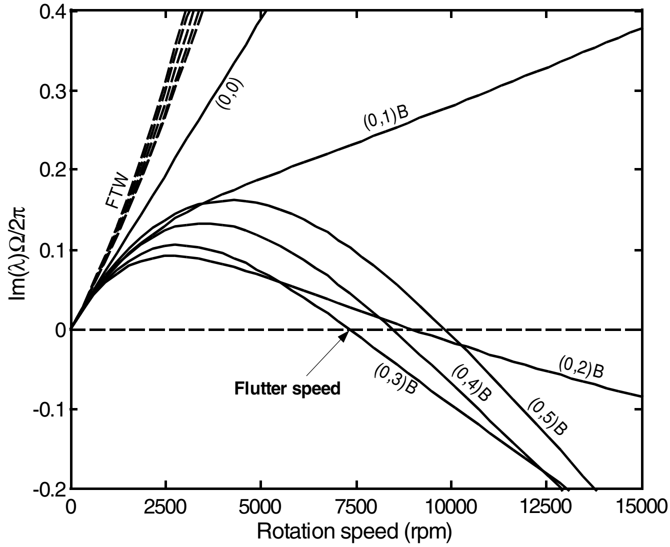

(a)

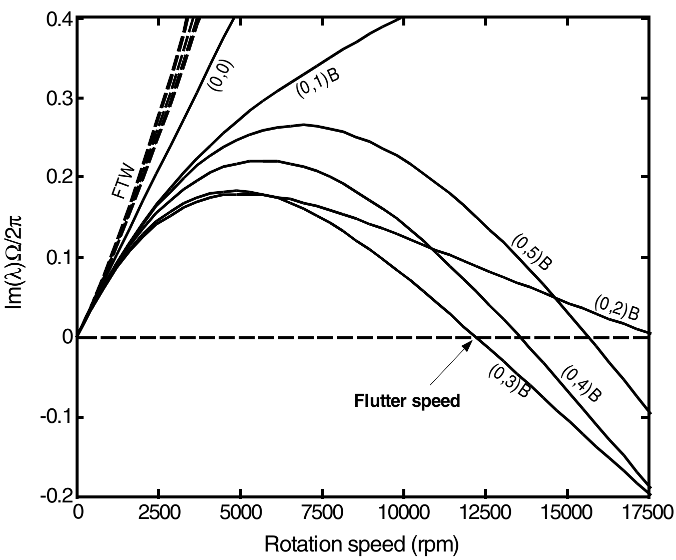

(b)

Fig. 6. Imaginary parts of the eigenvalues against the rotation speeds with $C = 0.01$ and $\Omega_d/\Omega = 0.85$ in the modeling: (a) for Disk-1 and (b) for Disk-2. The mode numbers (m, n) are indicated by the brackets.

the proposed simple model. The effect of the model parameters of damping coefficient C and the speed ratio Ω_d/Ω on mode frequencies (i.e. $\mathrm{Re}(\lambda)$) and dampings (i.e. $\mathrm{Im}(\lambda)$) of the rotating disk system have been evaluated. The simulations show that there are almost no differences on the mode frequencies for the different

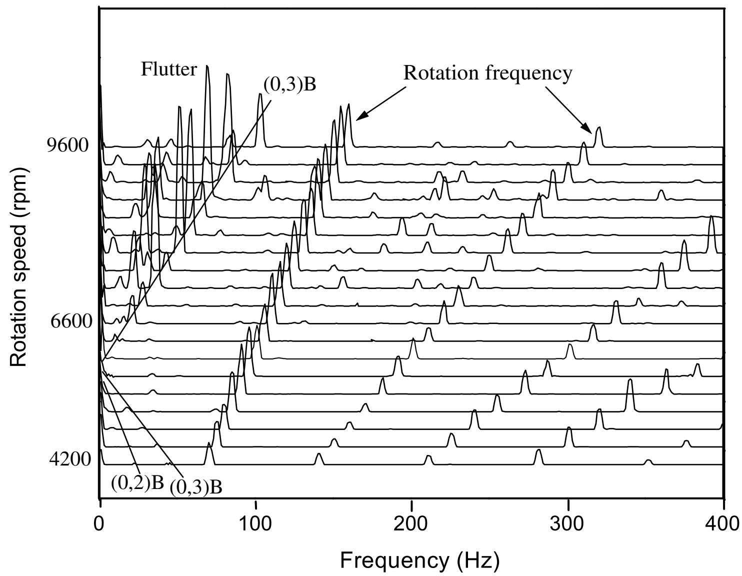

(a)

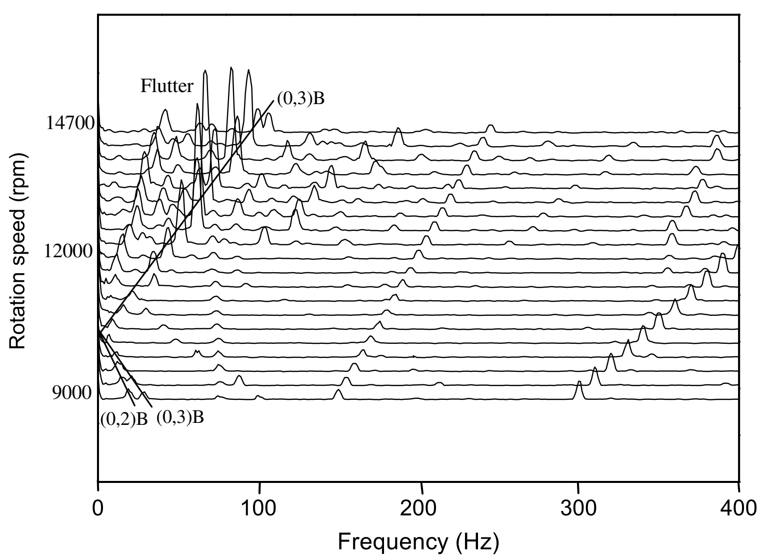

(b)

Fig. 7. Waterfall plots for (a) Disk-1 and (b) Disk-2 to observe the disk flutters and to estimate the flutter speeds.

damping coefficients C, and the mode frequencies of the rotating disk are not sensitive to the speed ratio $\Omega_{\mathrm{d}}/\Omega$. Figure 8(a) shows the influence of coefficient C on system dampings for Disk-1. It can be seen that the coefficient C only varies the amplitude of $\mathrm{Im}(\lambda)$ but there is no change to the flutter speed because the

Table 4. Flutter speeds (rpm) and frequencies (Hz) for flutter mode (0, 3)B.

Disk	Flutter Speed		Flutter Frequency	
	Predicted Result	Measured Result	Predicted Result	Measured Result
Disk-1	7300	∼7200	54	∼46
Disk-2	12200	∼12300	98	∼85

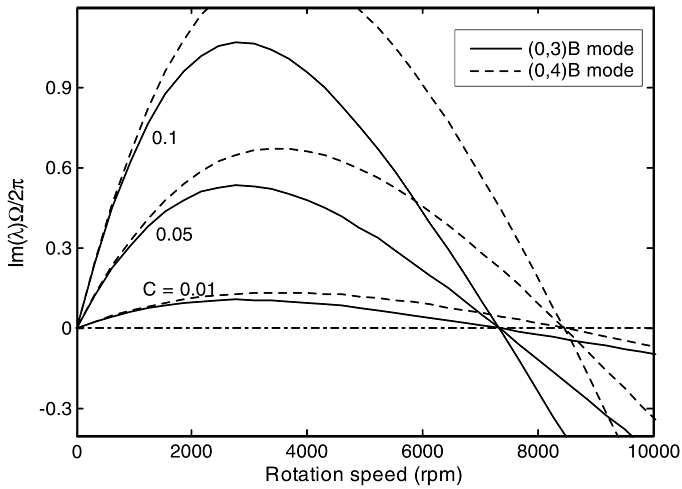

(a)

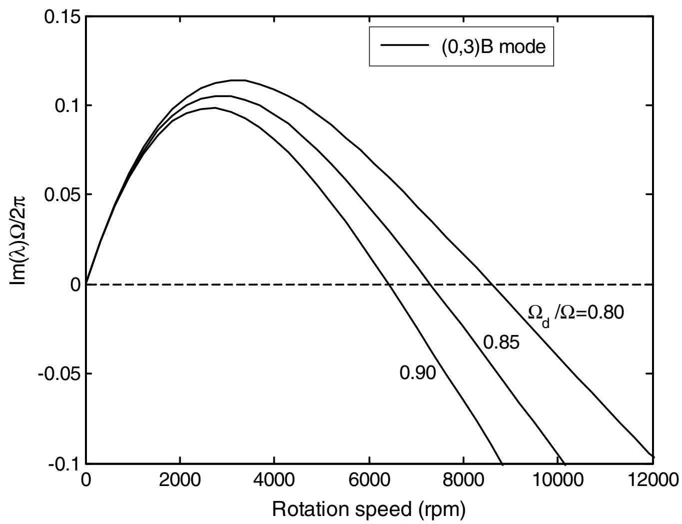

(b)

Fig. 8. Effect of the model coefficients on the system damping of Disk-1: (a) for different damping coefficient C with $\Omega_{\rm d}/\Omega = 0.85$, and (b) for different speed ratio $\Omega_{\rm d}/\Omega$ with $C = 0.01$.

damping curves switches from positive to negative at the same speed. However, the speed ratio $\Omega_{\rm d}/\Omega$, directly changes the flutter speed, as shown in Fig. 8(b) for mode $(0,3)$B. The smaller $\Omega_{\rm d}/\Omega$ is, the higher flutter speed will be. This suggests a technique for controlling the disk flutter if we know how to reduce $\Omega_{\rm d}/\Omega$ in the design of the disk system.

5. Conclusions

The flutters of rotating disks are numerically modeled, by using the empirical aerodynamic loading, to couple the disk vibrations with the surrounding air. The experiments on two steel disks with different diameters and thicknesses rotating between two rigid plates are conducted in order to measure the disk critical speeds and the flutter speeds. The aerodynamic loading proposed by Kim *et al.*[15] and Hansen *et al.*,[16] which is the source for the disk flutter, is further simplified with a fewer model parameters to predict the disk flutter by properly setting the damping coefficient, and especially the damping speed ratio $\Omega_{\rm d}/\Omega$. The simplification makes the model easier for evaluating the stability of rotating disks, which will assist in a better understanding and control of the rotating disk flutter. The simulation results on the critical speeds and the flutter speeds of rotating disks are compared with the experimental observations and the results are in reasonable agreement. It is confirmed that the disk flutter likely occurs on $(0,3)$B mode at the rotation speeds above the critical speed.

In the present study, we have noticed that the rotating disk flutter speed are sensitive to the speed ratio which has been set as $\Omega_{\rm d}/\Omega = 0.85$ and it works well for two disks with different geometries. Whether this is true in other cases will need further investigations. The studies on how the model parameter of speed ratio changes with a changing the gap between disk and support plates as well the fluid density around disk are expected to be carried by the authors in the near future.

Acknowledgments

The authors would like to acknowledge the fund supports provided by NCET-050878 and Lanzhou University, and the experimental support from CMMS of Nanyang Technological University.

Appendix

The application of the inner product on Eq. (12) with $R_{\rm ln}(r)e^{i(n\theta+\lambda t)}$, $(l = 0,1,\ldots,M_0)$ generates an acoustic force vector $[\mathbf{q}^{\rm a}]$ on the right-hand side. The elements for $[\boldsymbol{q}^{\rm a}]$ are

$$q_l^{\rm a} = 4\pi \int_{\kappa}^{1} \Lambda\lambda i \left[\sum_{k=1}^{\infty} d_k^{\rm a} \cosh(\alpha_k z_e) J_n(\xi_k r)\right] R_{\rm ln}(r) r dr. \tag{A.1}$$

The infinite series in the integrals are truncated at $k = K_0$, which is chosen as $K_0 = 30$ in our simulation showing acceptable precision. We introduce the following vectors:

$$[\mathbf{Y}] = [R_{0n}(r) \quad R_{1n}(r) \quad \cdots \quad R_{M_0 n}(r)]^{\mathrm{T}}, \quad [\mathbf{D}^{\mathrm{a}}] = [d_1^{\mathrm{a}} \quad d_2^{\mathrm{a}} \quad \cdots \quad d_{K_0}^{\mathrm{a}}]^{\mathrm{T}} \tag{A.2}$$

$$[\mathbf{\Phi}^{\mathrm{a}}] = [\cosh(\alpha_1 z_e) J_n(\xi_1 r) \quad \cosh(\alpha_2 z_e) J_n(\xi_2 r) \quad \cdots \quad \cosh(\alpha_{K_0} z_e) J_n(\xi_{K_0} r)] \tag{A.3}$$

and rewrite $[\mathbf{q}^{\mathrm{a}}]$ in the following form:

$$[\mathbf{q}^{\mathrm{a}}] = 4\pi\Lambda\lambda i \int_{\kappa}^{1} \{[\mathbf{Y}][\mathbf{\Phi}^{\mathrm{a}}][\mathbf{D}^{\mathrm{a}}]\} r dr. \tag{A.4}$$

Here, we give a detailed derivation on an explicit form for $[\mathbf{D}^{\mathrm{a}}]$ which is related to the disk vibrations, i.e. $[\mathbf{c}]$, through the boundary conditions. By substituting Eqs. (20) and (21) into the match condition (17), we have

$$\sum_{k=1}^{\infty} d_k^{\mathrm{a}} \alpha_k \sinh(\alpha_k z_e) J_n(\xi_k r) = 0, \quad \text{at } 0 \le r < \kappa, \tag{A.5}$$

$$-\sum_{k=1}^{\infty} d_k^{\mathrm{a}} \alpha_k \sinh(\alpha_k z_e) J_n(\xi_k r) = \sum_{m=0}^{M_0} c_m \lambda i R_{mn}(r), \quad \text{at } \kappa \le r \le 1, \tag{A.6}$$

$$\sum_{k=1}^{\infty} d_k^{\mathrm{a}} \cosh(\alpha_k z_e) J_n(\xi_k r) = 0, \quad \text{at } 1 < r \le r_e. \tag{A.7}$$

We take the finite terms of $k = 1, 2, 3, \ldots, K_0$ for the truncation of the infinite series in Eqs. (A.5)–(A.7) and choose finite points $r = r_j$ $(j = 1, 2, 3, \ldots, K_0)$ in the domain of $0 \le r \le r_e$ for approximate satisfaction of Eqs. (A.5)–(A.7). This leads to a set of equations

$$\begin{bmatrix}
\alpha_1 \sinh(\alpha_1 z_e) J_n(\xi_1 r_1) & \alpha_2 \sinh(\alpha_2 z_e) J_n(\xi_2 r_1) & \cdots & \alpha_{K_0} \sinh(\alpha_{K_0} z_e) J_n(\xi_{K_0} r_1) \\
\alpha_1 \sinh(\alpha_1 z_e) J_n(\xi_1 r_2) & \alpha_2 \sinh(\alpha_2 z_e) J_n(\xi_2 r_2) & \cdots & \alpha_{K_0} \sinh(\alpha_{K_0} z_e) J_n(\xi_{K_0} r_2) \\
\vdots & \vdots & \ddots & \vdots \\
\alpha_1 \sinh(\alpha_1 z_e) J_n(\xi_1 r_{K_0^1}) & \alpha_2 \sinh(\alpha_2 z_e) J_n(\xi_2 r_{K_0^1}) & \cdots & \alpha_{K_0} \sinh(\alpha_{K_0} z_e) J_n(\xi_{K_0} r_{K_0^1}) \\
-\alpha_1 \sinh(\alpha_1 z_e) J_n(\xi_1 r_{K_0^1+1}) & -\alpha_2 \sinh(\alpha_2 z_e) J_n(\xi_2 r_{K_0^1+1}) & \cdots & -\alpha_{K_0} \sinh(\alpha_{K_0} z_e) J_n(\xi_{K_0} r_{K_0^1+1}) \\
\vdots & \vdots & \ddots & \vdots \\
-\alpha_1 \sinh(\alpha_1 z_e) J_n(\xi_1 r_{K_0^1+K_0^2}) & -\alpha_2 \sinh(\alpha_2 z_e) J_n(\xi_2 r_{K_0^1+K_0^2}) & \cdots & -\alpha_{K_0} \sinh(\alpha_{K_0} z_e) J_n(\xi_{K_0} r_{K_0^1+K_0^2}) \\
\cosh(\alpha_1 z_e) J_n(\xi_1 r_{K_0^1+K_0^2+1}) & \cosh(\alpha_2 z_e) J_n(\xi_2 r_{K_0^1+K_0^2+1}) & \cdots & \cosh(\alpha_{K_0} z_e) J_n(\xi_{K_0} r_{K_0^1+K_0^2+1}) \\
\vdots & \vdots & \ddots & \vdots \\
\cosh(\alpha_1 z_e) J_n(\xi_1 r_{K_0}) & \cosh(\alpha_2 z_e) J_n(\xi_2 r_{K_0}) & \cdots & \cosh(\alpha_{K_0} z_e) J_n(\xi_{K_0} r_{K_0})
\end{bmatrix}$$

$$\times \begin{bmatrix} d_1^{\mathrm{a}} \\ d_2^{\mathrm{a}} \\ \vdots \\ d_{K_0^1}^{\mathrm{a}} \\ d_{K_0^1+1}^{\mathrm{a}} \\ \vdots \\ d_{K_0^1+K_0^2}^{\mathrm{a}} \\ d_{K_0^1+K_0^2+1}^{\mathrm{a}} \\ \vdots \\ d_{K_0}^{\mathrm{a}} \end{bmatrix} = \begin{bmatrix} 0 \\ 0 \\ \vdots \\ 0 \\ \sum_{m=0}^{M_0} c_m \lambda i R_{mn}(r_{K_0^1+1}) \\ \vdots \\ \sum_{m=0}^{M_0} c_m \lambda i R_{mn}(r_{K_0^1+K_0^2}) \\ 0 \\ \vdots \\ 0 \end{bmatrix}, \tag{A.8}$$

where K_0^1, K_0^2 and $K_0 - K_0^1 - K_0^2$ are the numbers of the chosen points in $0 \le r_j < \kappa$, $\kappa \le r_j \le 1$, and $1 < r_j \le r_e$, respectively. Equation (A.8) can be written in a matrix form

$$[\mathbf{A}^{\mathrm{a}}][\mathbf{D}^{\mathrm{a}}] = i\lambda[\mathbf{R}^{\mathrm{a}}][\mathbf{c}] \tag{A.9}$$

in which, $[\mathbf{R}^{\mathrm{a}}]$ is a $K_0 \times (M_0 + 1)$ matrix

$$[\mathbf{R}^{\mathrm{a}}] = \begin{bmatrix} & & 0 & \\ & & \vdots & \\ & & 0 & \\ R_{0n}(r_{K_0^1+1}) & R_{1n}(r_{K_0^1+1}) & \cdots & R_{M_0 n}(r_{K_0^1+1}) \\ R_{0n}(r_{K_0^1+2}) & R_{1n}(r_{K_0^1+2}) & \cdots & R_{M_0 n}(r_{K_0^1+2}) \\ \vdots & \vdots & \vdots & \vdots \\ R_{0n}(r_{K_0^1+K_0^2}) & R_{1n}(r_{K_0^1+K_0^2}) & \cdots & R_{M_0 n}(r_{K_0^1+K_0^2}) \\ & & 0 & \\ & & \vdots & \\ & & 0 & \end{bmatrix}. \tag{A.10}$$

From Eq. (A.9), we obtain

$$[\mathbf{D}^{\mathrm{a}}] = i\lambda[\mathbf{A}^{\mathrm{a}}]^{-1}[\mathbf{R}^{\mathrm{a}}][\mathbf{c}] \tag{A.11}$$

and substituting Eq. (A.11) into Eq. (A.4) yields

$$[\mathbf{q}^{\mathrm{a}}] = \left[-4\pi\Lambda\lambda^2 \int_{\kappa}^{1} \{[\mathbf{Y}][\mathbf{\Phi}^{\mathrm{a}}][\mathbf{A}^{\mathrm{a}}]^{-1}[\mathbf{R}^{\mathrm{a}}]\} r dr\right][\mathbf{c}] = [\mathbf{P}^{\mathrm{a}}][\mathbf{c}]. \tag{A.12}$$

References

1. G. Bouchard and F. E. Talke, Non-repeatable flutter of magnetic recording disks, *IEEE Trans. Mag.* **22**(5) (1986) 1019–1021.
2. I. Y. Shen, Vibration of flexible rotating disks, *Shock Vib. Dig.* **32**(4) (2000) 267–272.

3. A. A. Renshaw, C. D'Angelo and C. D. Mote Jr., Aerodynamically excited vibration of a rotating disk, *J. Sound Vib.* **177**(5) (1994) 577–590.
4. C. D'Angelo and C. D. Mote Jr., Aerodynamically excited vibration and flutter of a thin disk rotating at supercritical speed, *J. Sound Vib.* **168**(1) (1993) 15–30.
5. S. Y. Lee, J. D. Kim and S. Kim, Critical and flutter speeds of optical disks, *Microsyst. Technol.* **8** (2002) 206–211.
6. H. Hosaka and S. Crandall, Self-excited vibrations of a flexible disk rotating on an air film above a flat surface, *Acta Mechanica* **3** (1992) 115–127.
7. S. Chonan, Z. W. Jiang and Y. J. Shyu, Stability analysis of a $2''$ floppy disk drive system and the optimum design of the disk stabilizer, *J. Vib. Acoust.* **114**(2) (1992) 283–286.
8. F. Huang and C. D. Mote Jr., On the instability mechanism of a disk rotating close to a rigid surface, *J. Appl. Mech.* **62**(6) (1995) 764–771.
9. F. Huang and C. D. Mote Jr., Mathematical analysis of stability of a spinning disk under rotating arbitrarily large damping forces, *ASME J. Appl. Mech.* **118** (1996) 657–662.
10. G. Naganathan, S. Ramadhayani and A. K. Bajaj, Numerical simulations of flutter instability of a flexible disk rotating close to a rigid wall, *J. Vib. Contr.* **9**(1) (2003) 95–118.
11. M. Hansen, Aeroelasticity and dynamics of spinning disks, PhD thesis, Technical University of Denmark (1999).
12. C. O. Orgun and B. H. Tongue, On localization in coupled, spinning, circular plates, *ASME J. Vib. Acoust.* **116** (1994) 555–561.
13. J. S. Park and I. Y. Shen, Aerodynamically and structurally coupled vibration of multiple co-rotating disks, *ASME J. Vib. Acoust.* **126** (2004) 220–228.
14. K. Yasuda, T. Torii and T. Shimizu, Self-excited oscillations of a circular disk rotating in air, *JSME Int. J.* **35**(3) (1992) 347–352.
15. B. C. Kim, A. Raman and C. D. Mote Jr., Prediction of aeroelastic flutter in a hard disk drive, *J. Sound Vib.* **238**(2) (2000) 309–325.
16. M. H. Hansen, A. Raman and C. D. Mote Jr., Estimation of nonconservative aerodynamic pressure leading to flutter of spinning disks, *J. Fluids Struct.* **15**(1) (2001) 39–57.
17. S. Chonan, T. Mikami and H. Ishikawa, The vibration and critical speeds of rotating sawblades, *Proc. JSME*, Part C **52** (1985) 1805–1812 (in Japanese).
18. D. G. Jones (ed.), *Handbook of Viscoelastic Vibration Damping* (John Wiley & Sons, New York, 2001).